6. Theoretical calculation of the Makrofol responses to ^{222}Rn, ^{220}Rn and their progeny

Since the NTD response is a key parameter for the estimation of the airborne concentration of ^{222}Rn, ^{220}Rn and their decay products, attempts have, therefore, been made for its evaluation. Sensitivity determination of the NTDs can in principle be obtained experimentally by means of well-controlled and calibrated ^{222}Rn and ^{220}Rn exposure facilities. Nonetheless, these facilities are expensive and not easy to perform especially in the case of ^{220}Rn exposures, which only few laboratories possess. Hence, the theoretical calculations of the NTD sensitivities may be an useful solution.

6.1. Analytical method

In general, the track density per unit of time exposure for each NTD is the result of all α-emissions of ^{222}Rn, ^{220}Rn and their progeny able to produce observable tracks, and is given by

$$\dot{\rho}_m \ (\mathrm{cm}^{-2}\ \mathrm{h}^{-1}) = \sum_{n=1}^{7} \varepsilon^{\mathrm{v}}_{m,n} C_n + \sum_{n=1}^{7} \varepsilon^{\mathrm{d}}_{m,n} C^{\mathrm{d}}_n \tag{6.1}$$

where m labels the detector A, B, C and D (see Section 5.4),

$n = 1, 2, 3, 4, 5, 6, 7$ refers to the α-emitting nuclides ^{222}Rn, ^{218}Po, ^{214}Po, ^{220}Rn, ^{216}Po, ^{212}Bi, ^{212}Po, respectively,

$\varepsilon^{\mathrm{v}}_{m,n}$ and $\varepsilon^{\mathrm{d}}_{m,n}$ are the m-th detector sensitivity to n-th nuclide in the appropriate state: volume-distributed (v) and surface-deposited (d),

C_n is the concentration in Bq m^{-3} of the n-th nuclide that remains in airborne state, and

C_n^{d} (Bq m^{-3}) is the concentration of the n-th nuclide deposited on the housing walls of the diffusion chamber in the case of enclosed detectors (see the definition in Section 3.5).

Note that for the gas nuclides (^{222}Rn and ^{220}Rn) $C_1^{\mathrm{d}} = C_4^{\mathrm{d}} = 0$. These gases together with their airborne decay products are assumed to be homogeneously distributed in the considered air volume above the detector. Since with the energy windows used in this study all the detectors are insensitive to ^{222}Rn and ^{220}Rn progeny plated out directly on their surface, $\varepsilon_{m,n}^{\mathrm{d}}$ refers only to those progeny that are deposited on the inner housing walls of the enclosed detectors A and B. Thus, for the open detectors C and D, we have $\varepsilon_{\mathrm{C},n}^{\mathrm{d}} = \varepsilon_{\mathrm{D},n}^{\mathrm{d}} = 0$.

By assuming that all the solid angles subtended by any of detecting point areas do not vary with the position of these last, and that the α-tracks are uniformly distributed on the detector surface, the whole detector may approximate to a single point or *point like* detector and the volume-distributed detector sensitivity, $\varepsilon_{m,n}^{\mathrm{v}}$, can be obtained from the following expression (Fleischer, 1984)

$$\varepsilon_{m,n}^{\mathrm{v}} = \int_{V_{\mathrm{e}}} \frac{\cos\phi}{4\pi r^2}\, \mathrm{d}V \tag{6.2}$$

where ϕ is the α-particle angle of incidence related to the detector normal, r is the length of trajectory distance from the α-emission position down to the point like detector, and V_{e} is the effective volume. This last is defined for each n-th nuclide as the volume above the detector in which the emitted α-particles have a probability larger than zero to be recorded and is given by

$$V_{\mathrm{e}} = 2\pi \int_0^{\phi_{\mathrm{c}}} \int_{R_{\mathrm{min}}}^{R_{\mathrm{max}}} r^2 \sin\phi \; \mathrm{d}\phi \; \mathrm{d}r \tag{6.3}$$

According to this equation, the effective volume is limited by the detector critical angle, ϕ_{c}, above which α-particles entering its sensitive surface are not detected, and by the lower and upper effective ranges — R_{min} and R_{max}, respectively (see definition in Section 6.2.1) — and it may have different and complex geometric structures depending on the detector shape and size. Consequently, Equation (6.2) gives

$$\varepsilon_{m,n}^{\mathrm{v}} = \frac{1}{4} \int_0^{\phi_{\mathrm{c}}} \int_{R_{\mathrm{min}}}^{R_{\mathrm{max}}} \sin 2\phi \; \mathrm{d}\phi \; \mathrm{d}r \tag{6.4}$$

The solution of this equation is fairly complicated because of the functional form of the limits over which the integrals are taken. In principle, the critical angle is dependent on the energy of the emitted α-particles. In practice, these integrals are solved by neglecting this dependence for a first approximation (Fleischer, 1984; Somogyi et al., 1984; Dörschel and Piesch, 1993; Hadler and Paulo, 1994; Djeffal et al., 1997).

The upper limit of NTD volume-distributed sensitivities corresponds to an ideal detector that has any restriction neither on the α-particle angle of incidence ($\phi_c = \frac{\pi}{2}$) nor on its energy ($E_{min} = 0$ and $E_{max} = E_0$), i.e.,

$$\varepsilon^0_{m,n} = \frac{1}{4}\int_0^{\frac{\pi}{2}}\int_0^{R_0} \sin 2\phi \; \mathrm{d}\phi \; \mathrm{d}r = \frac{R_0}{4} \tag{6.5}$$

where R_0 is the full range in air of an α-particle whose initial energy is E_0.

In the case of ^{222}Rn and ^{220}Rn progeny that are uniformly deposited within the inner housing walls of the diffusion chambers used for the enclosed detectors A and B, the corresponding surface-deposited sensitivity is given by

$$\varepsilon^{\mathrm{d}}_{m,n} = \frac{\int_{S_e} \frac{\cos\phi}{4\pi r^2} \; \mathrm{d}S}{(\frac{S}{V})_{ch}} \tag{6.6}$$

where $(\frac{S}{V})_{ch}$ is the housing surface-to-volume ratio of the diffusion chamber used for the enclosed detectors and S_e is the effective surface, which is defined as the cross-section between the inner diffusion chamber's walls and the effective volume. The effective surface depends strongly on the inner housing shape and dimensions of the diffusion chamber. As the FzK diffusion chamber used in this study has a hemispherical shape with a radius R_{ch} (i.e., $r = R_{ch}$), we can write

$$S_e = 2\pi R^2_{ch}\int_0^{\phi_c} \sin\phi \; \mathrm{d}\phi \tag{6.7}$$

Taking into account this definition, Equation (6.6) becomes

$$\varepsilon^{\mathrm{d}}_{m,n} = \frac{1}{4}\frac{\int_0^{\phi_c} \sin 2\phi \; \mathrm{d}\phi}{(\frac{S}{V})_{ch}} \tag{6.8}$$

Analytical methods employing integral calculus over the effective volume and surface present difficulties in mathematical handling especially at varied detecting device geometry. In many cases they are limited only to a simple problem-specific geometry and to a single point detector. Furthermore, the analytical equations above cannot predict the non-uniform α-track distribution of the enclosed detector surface in which each point area may have different solid angle. Hence, different effective volume and surface depending on the diffusion chamber geometry. In this case, the detector response is obtained by summing all the partial volume-distributed and surface-deposited sensitivities found for all the point areas on the detector surface. This additional integral is not trivial and may complicate more the whole analytical calculation of the detector sensitivity.

6.2. Monte-Carlo method

Since α-decay is basically a stochastic process in which the direction and the time of emission are described by the laws of probability, numerical simulations of the NTD response using Monte-Carlo techniques should be a good alternative in front the analytical methods (Bonetti et al., 1991; Mirza et al., 1993; McLaughlin and Fitzgerald, 1994; Nikezic et al., 1995; Andriamanatena et al., 1997; Nourreddine et al., 1999; Sima, 2001). These simulations allow a wide variety in the parametric changes without requiring integration of a completely new analytical expression and they offer the possibility to be easily adapted to any detecting medium characteristics, size and geometry. In addition, they can take into account absorbers between the source and detector.

To simulate the α-particle emission, propagation and detection with the NTDs, a Monte-Carlo based computer program SIMAR (SImulation of the MAkrofol Response) has been developed. This program is written in Fortran[1] 90 and can be used on any personal computer system with a minimum CPU (Control Processor Unit) of Intel Pentium[2] of 100 MHz with at least 16 Mbytes of RAM (Random Access Memory) and an operating system of Windows[3] 95 (or higher). It can handle different NTDs as well as a variety of geometries including rectangular, cylindrical and spherical shape. A simplified flow chart of the SIMAR program is given in Figure 6.1. The calculation is performed by generating a number N of isotropic α-emissions or *histories* that occur within the effective volume or surface. The standard deviation in the result obtained after tracing N histories varies inversely proportional to $\sqrt{N}$. On the other hand, increasing the number of simulation demands a great amount of memory as well as computer time. For that reason, the cut-off criterion of the program, which was determined by a compromise between keeping under reasonable limits the computing time and statistical precision, is fixed to 5×10^5 successful histories, so that the number of simulations is kept variable in the range from $\sim4\times10^6$ to $\sim4\times10^8$ and the CPU time[4] needed to complete them is within $\sim$5 s and $\sim$9 min, respectively. The output parameters of the program are the volume-distributed or surface-deposited sensitivities for each nuclide of ^{222}Rn, ^{220}Rn and their α-active daughters, assuming that only atoms of this nuclide are present in the considered effective volume or surface. The relative uncertainties obtained using the law of error propagation and assuming a Poisson distribution probability are below 0.15%.

[1]Fortran (formula translator) is the first popular programming language which was created in 1957 by the International Business Machines (IBM) Corporation, USA.

[2]Manufactured by Intel Corporation, USA.

[3]The registered trade mark of Microsoft Corporation, USA.

[4]Obtained with an Intel Pentium IV of 1.6 kHz and 256 Mbytes RAM.

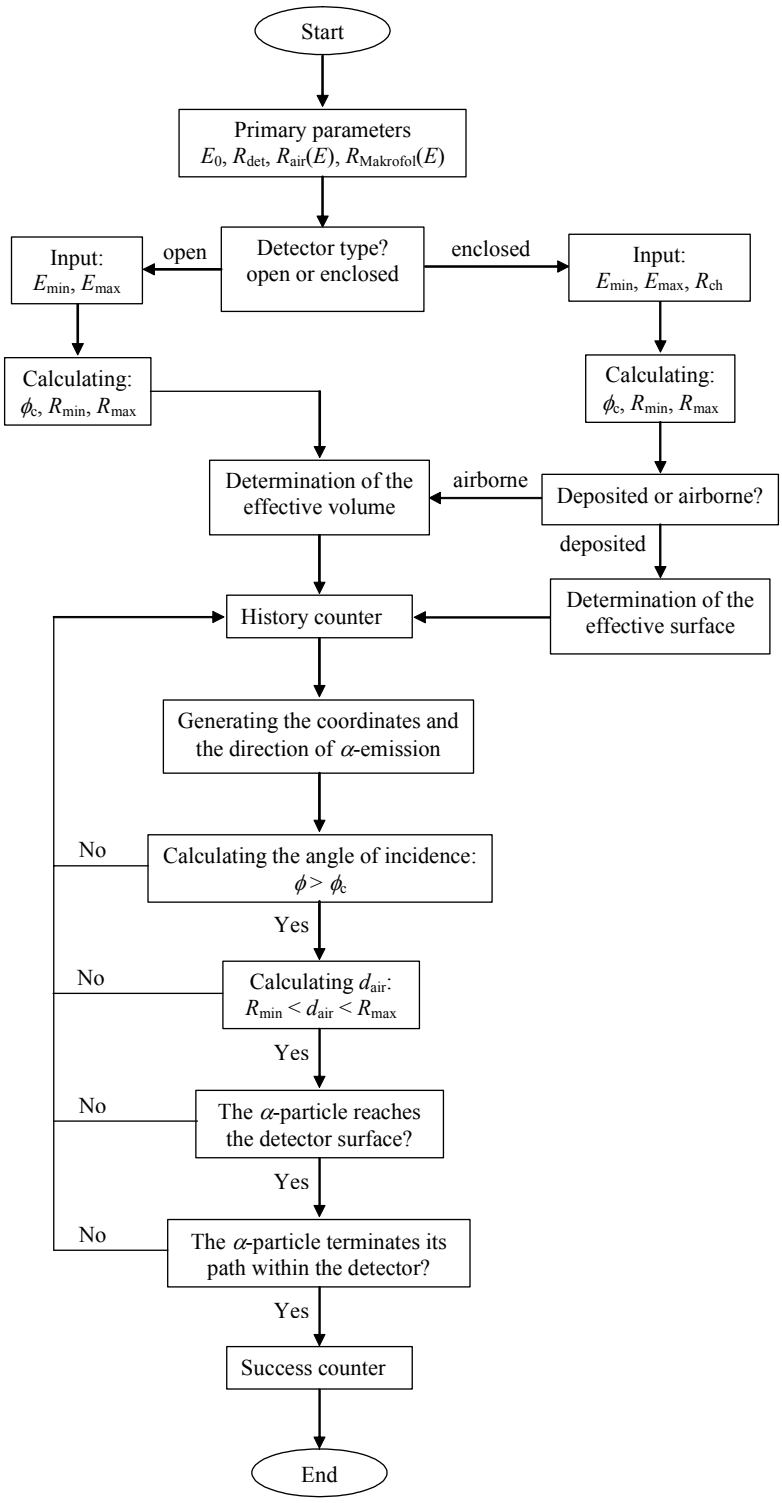

Figure 6.1. Flow chart of the SIMAR program.

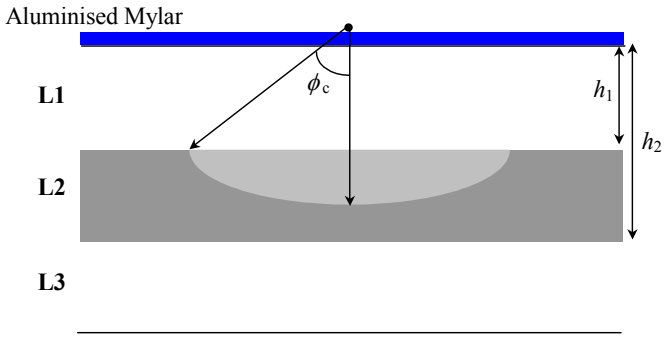

Figure 6.2. Schematic illustration of α-particle registration with electrochemical etched Makrofol detectors.

For the following considerations, it is useful to divide the electrochemically etched Makrofol detectors into three layers **L1, L2** and **L3** with respect to the energy window response for α-particle registration (see Figure 6.2):

1. Layer **L1** (from 0 to h_1) corresponds to the removed front layer of the detector during the pre-etching process along which all tracks produced by α-particles with energies below $E_{\min}$ are overetched, so that they cannot be enlarged by electric treeing process.

2. Layer **L2** (from h_1 to h_2) in which all α-particles with energies between $E_{\min}$ and $E_{\max}$ that terminate their path inside this layer will be transformed into electrochemically etch tracks.

3. Layer **L3** stands for the detector layer that remains unetched when finished the electrochemical etching process and has no importance along the simulation process.

According to all these considerations and as shown in Figure 6.2, we can write

$$h_1 = R_{\text{Makrofol}}(E_{\min} - 0.6) \text{ and } h_2 = R_{\text{Makrofol}}(E_{\max} - 0.6) \tag{6.9}$$

where $R_{\text{Makrofol}}(E)$ is the range in μm of α-particle with energy E (MeV) in Makrofol calculated from Equations (B.3) of the Appendix B. The value of 0.6 MeV, which is deduced from a previous study of our group (Baixeras et al., 1991) and confirmed using the Srim-2000 code, refers to the energy absorbed by the aluminised Mylar cover and it must be subtracted from any α-particle able to penetrate the Makrofol detector. In the subsequent, we present the details of the procedure adopted for the Makrofol detectors A, B, C and D.

6.2.1. Case of open detectors

In the case of the detector C and D response simulation, the history starts for each α-emission and for each α-emitter by assigning the following Cartesian coordinates $|x| \leq R_{\text{det}} + R_0$, $|y| \leq R_{\text{det}} + R_0$ and $z \leq R_0$, being R_{det} the detector radius, to a random position (**P**) related to an absolute reference system with origin at the detector centre as shown in Figure 6.3. Only α-particles originated within the effective volume are able to create tracks on the detector. For this reason, as a first step of simulation, the shape and size of the effective volume must be determined previously. This can be done by means of the rejection technique (Kalos and Whitlock, 1986) taking into account the detector critical angle, ϕ_{c}, to the detector normal above which α-particles are not recorded, and that the distance, d_{air}, from the point of emission (**P**) to the crossing point (**C**) on the detector plane, which is computed as $d_{\text{air}} = \frac{z}{\cos\phi}$, has to be between the lower and upper effective ranges, R_{min} and R_{max}. These last represent the distances from which α-particles arrive at the detector surface with energies ranging from E_{min} to E_{max}, and are calculated as

$$R_{\text{min}} = R_0 - R_{\text{air}}(E_{\text{max}}) \text{ and } R_{\text{max}} = R_0 - R_{\text{air}}(E_{\text{min}}) \tag{6.10}$$

where $R_{\text{air}}(E)$ is the range in cm of α-particle with energy E (MeV) in air whose expression is given by Equations (B.4) of the Appendix B; we have $R_0 = R_{\text{air}}(E_0)$. In turn, the critical angle is assumed to have a constant value of $\sim 45^o$ as stated by Bednár et al. (1998).

Once the starting point is within the effective volume, a direction of α-emission is chosen randomly towards an hemisphere down to the detector surface — $0 \leq \varphi \leq 2\pi$ and $\frac{\pi}{2} \leq \theta \leq \pi$, being φ and θ respectively the azimuthal and the zenith angles — so that its trajectory intersects the detector plane. This fact is taken into account when calculating the total activity multiplying the number N of α-emissions by a factor of 2. The description of the method used for the coordinate selection as well as for the direction of emission is explained in Appendix C. The next history step is to compare the angle of incidence ($\phi = \pi - \theta$) to its critical value ϕ_{c}. Any unsatisfied condition along the simulation process means that the particle is not detected and next position is generated after an increment in the history counter by unity. When the crossing point lies within the detector surface and since the range-energy relationships are found to be polynomial (see Appendix B), the residual energy is then calculated using the following expression

$$E'(\text{MeV}) = \frac{-0.297 + \sqrt{0.088 - 0.28(0.12 + d_{\text{air}} - R_0)}}{0.14} \tag{6.11}$$

Only values of the residual energy between E_{min} and E_{max} are considered. Finally, the coordinates of the trajectory end are tested to be sure that α-particle terminates its path within the detector. When all the conditions above are satisfied hence the α-particle is

detected and next position is generated after increasing both the track and history counters by unity. The volume-distributed sensitivity is, then, obtained as the ratio of number of successful histories or tracks (fixed above at 5×10^5) per unit of detector area to the number of α-emissions per unit effective volume.

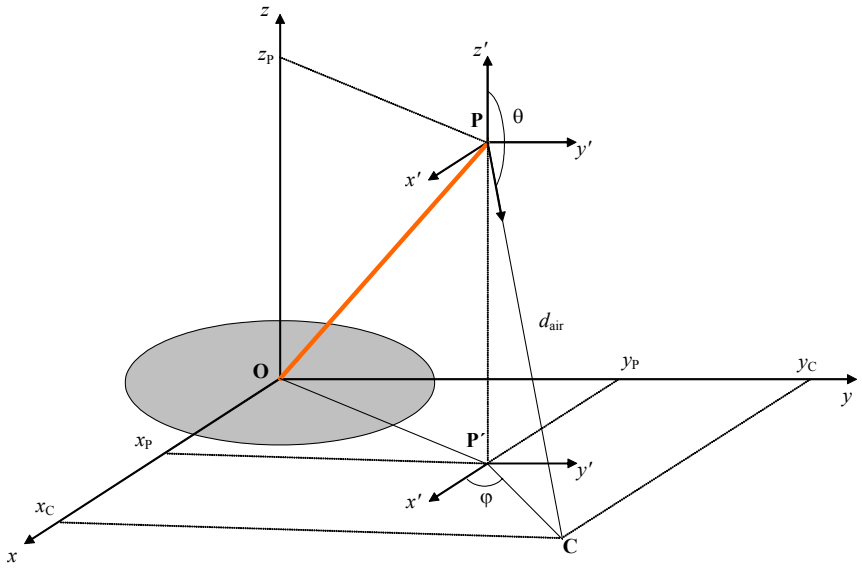

Figure 6.3. Representation of the α-emission in the considered airspace.

6.2.2. Case of enclosed detectors

In the case of the enclosed detectors A and B, the process of simulation is similar to that of the open detector C. However, their responses are limited by the inner housing walls of the diffusion chamber used. Only the part of the effective volume that is within the diffusion chamber housing is considered. Thus, it should be expected that, for the same concentrations of ^{222}Rn, ^{220}Rn and their α-active progeny in air, the volume-distributed sensitivity of the open detector C is higher than that obtained by the enclosed detectors A or B. For the deposited ^{222}Rn and ^{220}Rn α-emitter decay products, the only variance in the calculations is that the origin of α-emissions are chosen along the effective surface, by assuming an equal deposition probability on the whole inner walls of the FzK diffusion chamber. In this manner, the program calculates first the detection probability defined as the ratio of number of successful histories (5×10^5) per unit of detector area to the number of α-emissions per unit of effective surface. Then, the surface-deposited sensitivity is obtained by dividing the detection probability value to the surface-to-volume ratio, $(\frac{S}{V})_{\mathrm{ch}}$, of the FzK diffusion chamber.

6.2.3. Results of the calculations

Results of the effective volumes of ^{222}Rn, ^{220}Rn and their α-active progeny obtained by the SIMAR program for the two α-energy windows used in this study — [3.0 - 5.0] MeV and [6.3 - 7.5] MeV — are shown in Figures 6.4 and 6.5, respectively. As shown in Figure 6.4, only a fraction of the effective volume of ^{222}Rn, ^{218}Po, ^{220}Rn and ^{212}Bi (^{222}Rn+^{218}Po+^{220}Rn+^{212}Bi in the case of detector A and only ^{222}Rn+^{218}Po in the case of detector B) may result into α-particle registration when using the FzK diffusion chamber and an energy window [3.0 - 5.0] MeV, while, there is no possibility for ^{214}Po, ^{216}Po and ^{212}Po detection. This is because of the high energy of their α-emissions. In addition, the ^{218}Po and ^{212}Bi that deposit on the inner housing walls may contribute to the enclosed detector reading (^{218}Po+^{212}Bi in the case of detector A and ^{218}Po in the case of detector B). For detector C, all of ^{222}Rn, ^{220}Rn and their α-emitter progeny are able to be detected. According to Figure 6.5, only the ^{214}Po, ^{216}Po and ^{212}Po are able to be recorded by the detector D since the lower threshold limit of this last is below the initial energies of their α-emissions. The theoretical $\varepsilon^{\mathrm{v}}_{m,n}$ and $\varepsilon^{\mathrm{d}}_{m,n}$ values calculated for the detectors A, B, C and D in front of ^{222}Rn, ^{220}Rn and their α-emitter progeny are given in Table 6.1. In this table, since the mean lives of ^{216}Po and ^{212}Po are too short to be detected, their α-energies (6.78 MeV in the case of ^{216}Po and 8.78 MeV in the case of ^{212}Po) are assigned to their precursors ^{220}Rn and ^{212}Bi, respectively.

Essentially, the inner hemispherical housing of the enclosed detectors A and B may be considered as an unventilated small enclosure space into which ^{222}Rn and/or ^{220}Rn diffuse and within which the aerosol particles do not take place. Therefore, their progeny may be found only in the airborne-unattached state within the FzK diffusion chamber and the steady-state Equations (3.17), (3.18) and (3.19) describing the partitioning of ^{222}Rn and ^{220}Rn progeny concentration within a reference room are also applied to these detectors.

As the surface-to-volume ratio, $(\frac{S}{V})_{\mathrm{ch}}$, of the FzK diffusion chamber is equal to 300 m^{-1}, the corresponding deposition rate for airborne-unattached ^{222}Rn and ^{220}Rn progeny, $\lambda^{\mathrm{u,ch}}_{\mathrm{d}}$, according to respective deposition velocities given in Section 3.3, may range from 5.4×10^{2} h^{-1} to 5.4×10^{3} h^{-1}. These values are much higher and should dominate the ^{222}Rn and ^{220}Rn daughters' behaviour inside the FzK diffusion chamber ensuring a complete (100%) deposition of their atoms on its inner surface. Indeed, this behaviour was confirmed using the same procedure as in Section 5.3.1 and assuming all the possible values for $\lambda^{\mathrm{u,ch}}_{\mathrm{d}}$. Accounting for this and for the results presented in Table 6.1, the response equations of the detectors A, B, C, and D can be rewritten as

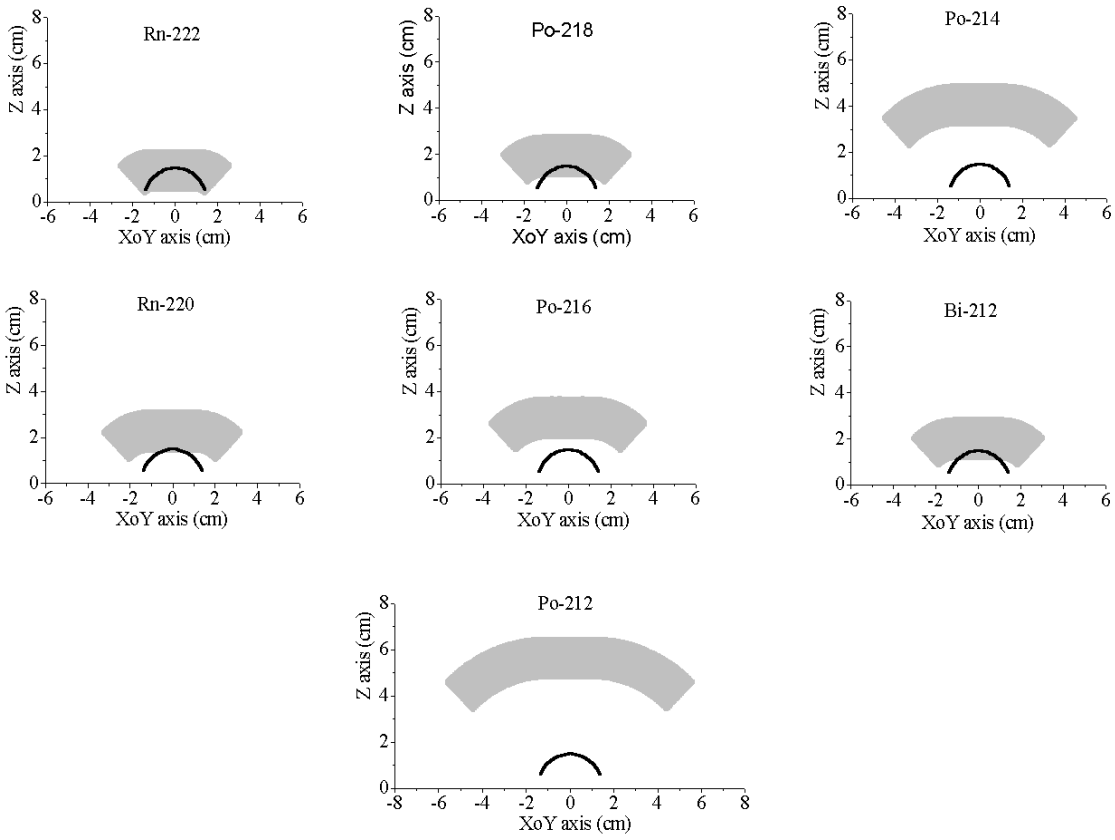

Figure 6.4. The effective volumes of ^{222}Rn, ^{220}Rn and their α-active progeny obtained for the α-energy window [3.0 - 5.0] MeV, the black line illustrates the cross-section between the effective volume and the hemispherical housing in the case of detectors A and B.

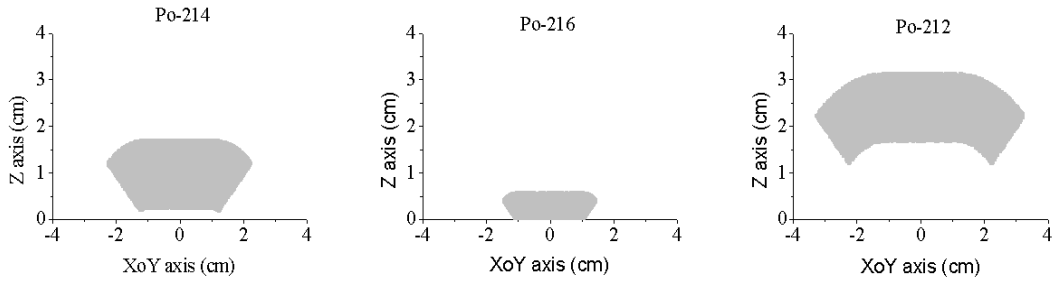

Figure 6.5. The effective volume of ^{222}Rn, ^{220}Rn and their α-active progeny obtained for the α-energy window [6.3 - 7.5] MeV.

Table 6.1. Characteristics of α-emissions ^{222}Rn, ^{220}Rn and their progeny and the calculated $\varepsilon^{\mathrm{v}}_{m,n}$ and $\varepsilon^{\mathrm{d}}_{m,n}$ values for the detectors A, B, C and D.

	Detector	^{222}Rn	^{218}Po	^{214}Po	^{220}Rn		^{212}Bi	
E_0 (MeV)		5.49	6.00	7.69	6.29	6.78	6.07	8.78
Branching ratio		1	1	1	1	1	0.36	0.64
$\varepsilon^{\mathrm{v}}_{m,n}$	A	0.38	0.10	0.00	0.01	0.00	0.07	0.00
($\mathrm{cm^{-2}\ kBq^{-1}\ m^3\ h^{-1}}$)	B	0.38	0.10	0.00	NP	NP	NP	NP
	C	0.74	0.71	0.66	0.69	0.68	0.70	0.65
	D	0.00	0.00	0.66	0.00	0.26	0.00	0.59
$\varepsilon^{\mathrm{d}}_{m,n}$	A	0.00	0.38	0.00	0.00	0.00	0.37	0.00
($\mathrm{cm^{-2}\ kBq^{-1}\ m^3\ h^{-1}}$)	B	0.00	0.38	0.00	NP	NP	NP	NP
% deposited within the FzK inner surface		0	100	100	0	0	100	100

NP: not present

$$\dot{\rho}_{\mathrm{A}} = 0.38C^{\mathrm{ch}}_{^{222}\mathrm{Rn}} + 0.38C^{\mathrm{d,ch}}_{^{218}\mathrm{Po}} + 0.01C^{\mathrm{ch}}_{^{220}\mathrm{Rn}} + 0.13C^{\mathrm{d,ch}}_{^{212}\mathrm{Bi}} \quad (6.12)$$

$$\dot{\rho}_{\mathrm{B}} = 0.38C^{\mathrm{ch}}_{^{222}\mathrm{Rn}} + 0.38C^{\mathrm{d,ch}}_{^{218}\mathrm{Po}} \quad (6.13)$$

$$\dot{\rho}_{\mathrm{C}} = 0.74C_{^{222}\mathrm{Rn}} + 0.71C_{^{218}\mathrm{Po}} + 0.66C_{^{214}\mathrm{Po}} + 1.37C_{^{220}\mathrm{Rn}} + 0.67C_{^{212}\mathrm{Bi}} \quad (6.14)$$

$$\dot{\rho}_{\mathrm{D}} = 0.66C_{^{214}\mathrm{Po}} + 0.26C_{^{220}\mathrm{Rn}} + 0.38C_{^{212}\mathrm{Bi}} \quad (6.15)$$

where C^{ch}_n denotes the value of the n-th nuclide inside the diffusion chamber, while the C_n stands for its actual indoor concentration. As inside the FzK diffusion chamber ^{222}Rn and ^{220}Rn are in equilibrium with their decay products, i.e., $C^{\mathrm{ch}}_{^{222}\mathrm{Rn}} = C^{\mathrm{d,ch}}_{^{218}\mathrm{Po}}$ and $C^{\mathrm{ch}}_{^{220}\mathrm{Rn}} = C^{\mathrm{d,ch}}_{^{212}\mathrm{Bi}}$, Equations (6.12) and (6.13) become

$$\dot{\rho}_{\mathrm{A}} = 0.76C^{\mathrm{ch}}_{^{222}\mathrm{Rn}} + 0.14C^{\mathrm{ch}}_{^{220}\mathrm{Rn}} \quad (6.16)$$

$$\dot{\rho}_{\mathrm{B}} = 0.76C^{\mathrm{ch}}_{^{222}\mathrm{Rn}} \quad (6.17)$$

For the open detectors C and D, and as shown in Equations (6.14) and (6.15), their response is also influenced by the presence of airborne ^{212}Bi. However, as shown in Section 5.3.1, this presence do not exceed in the worse cases 4% of the actual ^{220}Rn concentration. If we attribute all the tracks produced by the airborne ^{212}Bi to that of ^{220}Rn, the overestimation in the concentration of this last will not exceed 2% in the case of the detector C and 6% in the case of the detector D. This overestimation is minimal, 0.5% in the case of the detector C and 1.5% in the case of the detector D, if we consider only

the geometric mean value of the ^{212}Bi disequilibrium degree (see Table 5.1). Therefore, the contribution of the eventual presence of airborne ^{212}Bi in the equations given the responses of the detectors C and D can be ignored and we have

$$\dot{\rho}_{\mathrm{C}} = 0.74C_{^{222}\mathrm{Rn}} + 0.71C_{^{218}\mathrm{Po}} + 0.66C_{^{214}\mathrm{Po}} + 1.37C_{^{220}\mathrm{Rn}} \quad (6.18)$$

$$\dot{\rho}_{\mathrm{D}} = 0.66C_{^{214}\mathrm{Po}} + 0.26C_{^{220}\mathrm{Rn}} \quad (6.19)$$

According to Equations (6.16), (6.17), (6.18) and (6.19), the airborne concentrations of ^{222}Rn, ^{220}Rn, ^{218}Po and ^{214}Po can be obtained if the track densities of the detectors A, B, C and D are well-known.

6.2.4. Test validation

To test the accuracy of the program SIMAR, we have simulated the response of an open ideal detector ($\phi_{\mathrm{c}} = \frac{\pi}{2}$, $E_{\min} = 0$ and $E_{\max} = E_0$) in front ^{222}Rn, ^{220}Rn and their α-active decay products. The volume-distributed sensitivity values were validated with respect to analytical predictions of Equation (6.5). The results of this validation are given in Table 6.2. As shown in this table, the two methods give values very close to each other. The percent deviations obtained by the Monte-Carlo simulation are from 0.00% to 0.41%.

Nevertheless, being certain that this agreement is not sufficient to test the validity of the algorithmic procedures used in the SIMAR program, we have resimulated the response of the same ideal detector but enclosed within a FzK diffusion chamber. To contrast the results obtained by our program, a Surface Barrier Detector (SBD) — assumed here to behave as an ideal detector — was positioned exactly in the same position as normally occupied by an enclosed Makrofol detector within the FzK diffusion chamber (see Figure 6.6) and the conjunct were exposed to a ^{222}Rn-rich atmosphere. With the SBD connected to a multi-channel pulse analyser, it is possible to perform α-spectrometry with a good energy resolution. An example of a typical α-spectrum measured with the SBD inside the FzK diffusion chamber itself exposed to indoor ^{222}Rn-bearing air is shown in Figure 6.7.

Table 6.2. Comparison of the SIMAR program predictions with analytical method for an open ideal detector.

		$\varepsilon^{v}_{m,n}$ (cm^{-2} kBq^{-1} m^{3} h^{-1})		
Radionuclide	E_0 (MeV)	Equation (6.5)	SIMAR	% deviation*
^{222}Rn	5.49	3.48	3.49	0.29
^{218}Po	6.00	3.98	3.98	0.00
^{214}Po	7.69	5.89	5.91	0.17
^{220}Rn	6.29	4.27	4.27	0.00
	6.78	4.82	4.83	0.21
^{212}Bi	6.07	4.04	4.05	0.25
	8.78	7.31	7.28	0.41

* calculated as $\left|\frac{\text{SIMAR} - \text{Eq. (6.5)}}{\text{Eq. (6.5)}}\right| \times 100$

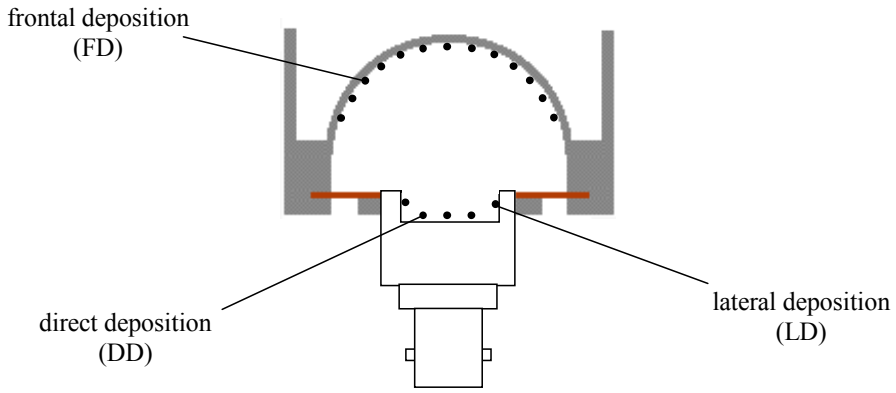

Figure 6.6. Enclosed SBD within the FzK diffusion chamber.

Similarly, the SIMAR program was adapted to give as an output parameter the energy deposited on the detector as a result of α-emissions from ^{222}Rn and its progeny inside the diffusion chamber. Figure 6.8 shows the computed α-energy distributions, in steps of 0.1 MeV, of individual nuclides of ^{222}Rn and its decay products as well as the resulting α-spectrum for an ideal detector within the FzK diffusion chamber.

In the simulation, all the ^{222}Rn daughters were supposed to be completely and uniformly deposited on the inner walls of the diffusion chamber as well as on the detector surface itself. For a direct comparison, both measured and computed α-spectrum were normalised to the integral of the corresponding spectra and the ordinates are given in %. We should point out that a perfect knowledge of the detector shape and size as well as its exact

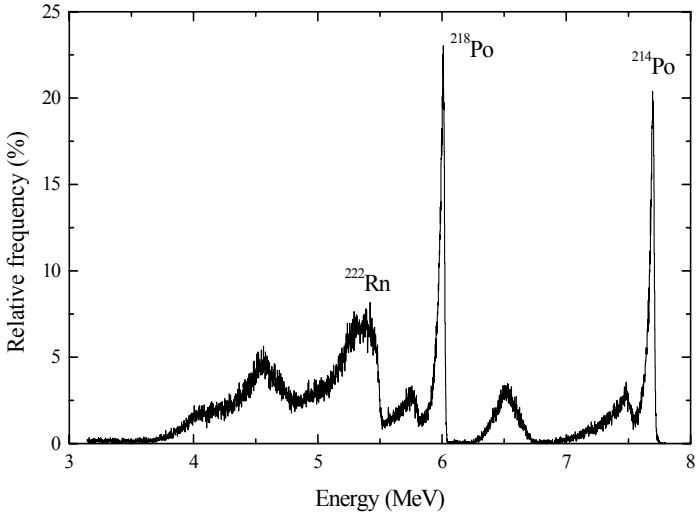

Figure 6.7. Typical α-spectrum measured with the SBD inside the FzK diffusion chamber in a ^{222}Rn-rich atmosphere.

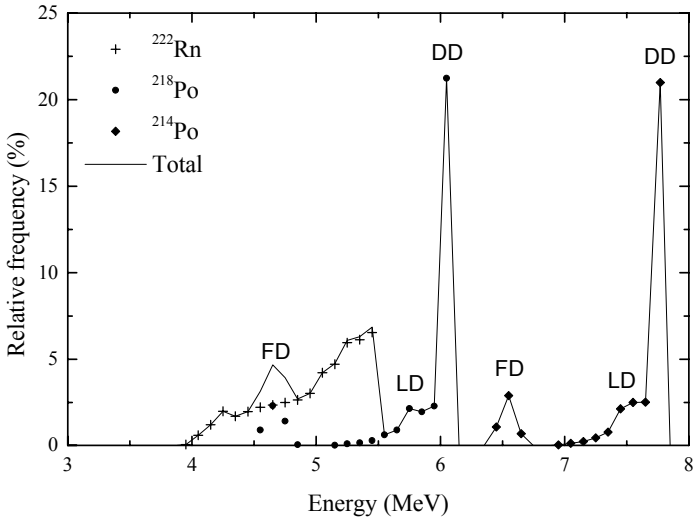

Figure 6.8. Computed α-energy distributions of ^{222}Rn and its progeny as well as the resulting α-spectrum for an ideal detector within the FzK diffusion chamber. FD, LD and DD are defined in the text.

position within the FzK diffusion chamber are of great importance since any little variation of these parameters may change considerably the computed α-spectrum. According to the SIMAR predictions, each of the two polonium isotopes presents three peaks:

1. the DD peak, which corresponds to the initial energy of α-emission (6.00 MeV in the case of ^{218}Po and 7.67 MeV in the case ^{214}Po) as a consequence of a direct deposition of these isotopes on the detector surface (see Figure 6.6),

2. the LD peak that takes into account the ^{222}Rn daughter deposition process on the lateral surface of the SBD, and

3. the FD peak showing the contribution of deposited α-active nuclide onto the hemispherical surface in front of the detector.

In contrast to ^{218}Po and ^{214}Po, ^{222}Rn does not have a clearly expressed peak because its atoms are homogeneously distributed in the entire volume of the FzK diffusion chamber. As clearly shown in Figures 6.7 and 6.8, there is a satisfactory agreement between the computed α-spectrum and that measured with the SBD. The SIMAR program have succeed in reproducing a similar response as that obtained by the SBD. This fact confirms the essential correctness of the assumption of a complete (100%) deposition of ^{222}Rn progeny within the FzK diffusion chamber.